JOURNAL OF THERMOPHYSICS AND HEAT TRANSFER
Vol. 10, No. 4, October–December 1996

Injection Cooling of Blunt Bodies Flying at High Mach Numbers

Sreekanth* and N. M. Reddy†
Indian Institute of Science, Bangalore-560 012, India

A study of transpiration cooling of blunt bodies such as a hemicylinder is made by solving Navier–Stokes equations. An upwind, implicit time-marching code is developed for this purpose. The study is conducted for both perfect-gas and real-gas (chemical equilibrium) flows. Investigations are carried out for a special wall condition that is referred to as no net heat flow into the wall condition. The effects of air injection on wall temperature are analyzed. Analyses are carried out for Mach numbers ranging between 6–10 and Reynolds numbers ranging between 10^6–10^7. Studies are made for spatially constant as well as spatially varying mass injection rate distributions. While cold air injection reduces the wall temperature substantially, transpiration cooling is relatively less effective when the gas is in chemical equilibrium.

Introduction

COOLING of external surfaces of a vehicle flying at hypersonic Mach numbers is a very crucial and challenging task because of the enormity of the heat load to which these vehicles are subjected. Cooling of such surfaces by injecting cold gas through a porous surface (transpiration cooling) is one among very few potential candidates for cooling such vehicles.[1] The theoretical analyses made in the area of transpiration cooling are based on approximate equations, and hence, have their own advantages (simplicity) and disadvantages (questionable validity).[2–4] Recently, Sreekanth and Reddy[2,3] studied transpiration cooling over a flat plate by solving the Navier–Stokes equations. The study of Refs. 2 and 3 was limited to chemically inert flows with spatially constant mass injection rates.

The objective of the present work is to perform the analyses of transpiration cooling for a practically more useful geometry (than the flat plate) such as a hemicylinder (Fig. 1). In spite of being two dimensional in nature, flow over a hemicylinder has applications in the leading edge of a delta wing and the lip of an engine cowling. Additionally, studies have also been made with chemically equilibrium flows and spatially varying mass injection rates. The study has been made using no net heat transfer to the wall condition.[2–4] The implication of such a boundary condition is that the wall temperature is obtained as a part of the solution for a given value of the coolant temperature (more likely to be known in reality), mass injection rate, and the freestream conditions. This is in contrast to the earlier studies where the wall was considered to be isothermal with a prescribed wall temperature.

Numerical Algorithm

The system of governing equations that consists of continuity, two-momentum, and energy equations can be written in integral form for a control volume of area A (two dimensional) as follows:

$$\frac{\partial \bar{U}}{\partial t} + \frac{1}{A}\int_S \boldsymbol{F}\cdot\boldsymbol{n}\,\mathrm{d}S = 0 \tag{1}$$

where $\bar{U}$ is the averaged value of the conserved vector and the integral term represents the net flux of the conserved variables crossing the control volume. The expressions for these variables are amply available in the literature. Equation (1) coupled with the equation of state and Sutherland's law for the viscosity coefficient forms a closed set of nondimensionalized equations. The coordinates are nondimensionalized by the radius of the hemicylinder, velocities by the freestream velocity, pressure by twice the freestream dynamic pressure, and temperature and density by freestream temperature and density, respectively. Also, the coefficient of viscosity is nondimensionalized by its freestream value. The governing equations are discretized in the finite volume formulation. The convective terms in the equations are evaluated using van Leer's[5] scheme and MUSCL extrapolation[6] with $\kappa = \frac{1}{3}$ to enhance the

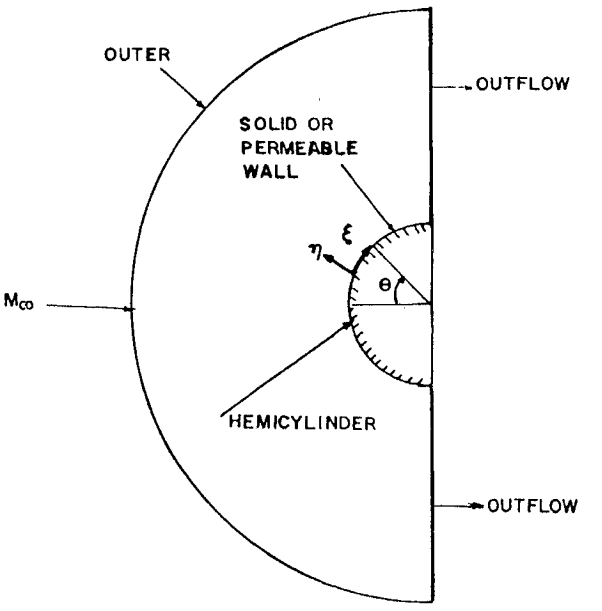

Fig. 1 Body geometry.

Presented as Paper 95-2082 at the AIAA 29th Thermophysics Conference, San Diego, CA, June 19–22, 1995; received July 10, 1995; revision received Jan. 20, 1996; accepted for publication March 21, 1996.

*Research Associate, Department of Aerospace Engineering; currently Ph.D. Fellow, McGill University, Montreal, Canada.

†Professor, Department of Aerospace Engineering. Associate Fellow AIAA.

accuracy. The viscous terms are calculated using the auxiliary cell approach.[7] The equations are time marched using the Euler-implicit method. The Line–Jacobi relaxation algorithm is used for simplifying the resulting equations.

Various boundaries encountered in this work are presented in Fig. 1. The outer boundary is chosen such that the freestream conditions exist there. On the outflow boundaries, quantities are extrapolated from the interior. This is valid if the flow is supersonic outside the boundary layer. On the solid (or permeable) wall, the half-cell approach of Liou[8] is used, which demands the conserved quantities on the solid (or permeable) boundary instead of their derivatives. In the absence of gas injection, the velocities on the walls are zero. Adiabatic wall condition is used to determine the wall temperature. The pressure is obtained by solving the normal momentum equation written in the body-fitted coordinate system (ξ, η) on the wall (Fig. 1). The density is obtained using the equation of state. In the presence of gas injection, the mass flux tangential to the wall surface is set to zero and the mass flux normal to the wall surface ($\dot{m}_w$) is known. The wall temperature is determined using the no net heat transfer to the wall condition.[2,3] This condition leads to

$$\frac{\mu}{Re_\infty Pr}\frac{\partial T}{\partial \eta} = \dot{m}_w(T_w - T_c) \tag{2}$$

Here μ is the viscosity coefficient, Re_∞ is the Reynolds number based on the cylinder radius, Pr is the Prandtl number, T is the temperature, and η is the distance normal to the surface. The subscripts w and c refer to the wall and the coolant conditions, respectively. Investigations are also made in this article to determine the mass injection rate required to have a desired isothermal wall. Equation (2) is used in such a case to determine the mass injection rate for a given wall temperature.

Implicit Boundary Conditions

The final form of the numerical algorithm can be written as follows:

$$(L)_{ij}\Delta\bar{U}_{ij-1} + [(I/\Delta t) + M]_{ij}\Delta\bar{U}_{ij} + (N)_{ij}\Delta\bar{U}_{ij+1} = R_{ij} \tag{3}$$

where L, M, and N are the Jacobian matrices.[4] Here i and j are the cell indices in ξ and η directions. When Eq. (3) is applied at $j = j_{\max} - 1$ ($j_{\max}$ is the maximum number of cells in the η direction), it requires the solution change ($\Delta\bar{U}$) at location (i, $j_{\max}$), which is zero since the freestream condition always exists on this boundary. Similarly the solution change is required on the $j = 1$ boundary also. In such a case, the solution change is expressed in terms of the solution change of interior points as follows:

$$\Delta\bar{U}_{i1} = (X)\Delta\bar{U}_{i2} \tag{4}$$

and this expression is incorporated into Eq. (3) at $j = 2$. The matrix X is different for different wall conditions such as adiabatic or isothermal or whether gas is injected or not. The details of the derivations of the square matrix X are available in Ref. 4 and are not given here to conserve space.

Equilibrium Chemistry

In the present work the species O, N, O^+, N^+, e^-, O_2, N_2, NO, and NO^+ were used with the following set of chemical reactions:

$$\begin{gathered} O_2 \rightleftharpoons O + O, \quad N_2 \rightleftharpoons N + N, \quad O \rightleftharpoons O^+ + e, \quad N \rightleftharpoons N^+ + e^- \\ NO \rightleftharpoons N + O, \quad N + O \rightleftharpoons NO^+ + e^- \end{gathered} \tag{5}$$

When the flow is in chemical equilibrium, the governing equations remain the same as that of the perfect gas case, except for the terms representing the energy transport in the species diffusion equation. For example, the heat flux term in the x direction looks like

$$\dot{q}_x = -\frac{k}{(\gamma_\infty - 1)Pr_\infty Re_\infty M_\infty^2}\frac{\partial T}{\partial x} - \sum_{n=1}^{NS}\frac{\rho D_{nm}}{Re_\infty Sc}\frac{\partial C_n}{\partial x}h_n \tag{6}$$

Here k is the thermal conductivity, M_∞ is the freestream Mach number, ρ is the density, Sc is the Schmidt number, C_n is the mass fraction of a species n, h_n is the specific enthalpy of the species, and NS is the total number of species. The equation of state that relates the thermodynamic quantities is not available in the closed form when the flow is in chemical equilibrium. The mixture transport properties depend on the mole fractions and the species transport properties. With the knowledge of the species transport properties and mole fractions, the mixture transport properties can be obtained using Wilke's mixture rule.[9] The species transport properties are obtained by fitting a curve to the tabulated data of Svehla.[10] The multicomponent diffusion coefficient can be obtained by solving a system of species conservation equations. Since this is a very complicated procedure, in the present work the following empirical relation suggested by Anderson[11] is used:

$$D_{nm} = (1 - X_n)\Big/\sum_{l=1}^{NS}\frac{X_l}{D_{nl}} \tag{7}$$

where D_{nl} is the binary diffusion coefficient that is given by the following equation:

$$D_{nl}^* = 0.0018583\frac{\sqrt{(T^*)^2[(M_n + M_l)/M_nM_l]}}{p^* d_{nl}^2 \Omega_{d,nl}} \tag{8}$$

and M is the molecular weight. The quantities T^*, d_{nl}, and the collision integral $\Omega_{d,nl}$ can be obtained from Ref. 10.

The numerical algorithm used in the chemical equilibrium flows is almost the same as that of the perfect gas model. The modified van Leer's scheme[12] is used here to account for nonconstant γ. The difficulty comes in relating the thermodynamic quantities. Applying the law of mass action to the chemical reactions [Eq. (5)], a set of equations will result. These equations can be solved for the mass fractions as a function of two independent thermodynamic quantities. With the knowledge of two thermodynamic quantities and the mass fraction of each species, it is possible to get any other thermodynamic quantity. Thermodynamic quantities are needed not only at the cell centers, but also at the cell interfaces for the calculation of the fluxes using van Leer's scheme. This means that an elaborate set of equations needs to be solved twice at each interface of a cell apart from the cell centers. Also, van Leer's scheme requires the speed of sound that depends on the derivatives of the thermodynamic quantities that cannot be obtained by this method. Hence, the curve fits developed by Tannehill and Mugge[13] for obtaining pressure, temperature, and speed of sound as a function of density and internal energy are used in the present work. With this the mass fractions of the species are needed only at the cell centers to calculate the mixture transport properties. For this, the system of equations resulting from the law of mass actions is solved for given values of density and temperature. Though the curve fits are available for the transport properties such as μ and k of equilibrium air, the diffusion heat flux term in Eq. (6) can be calculated only with the knowledge of mass fractions of each species. The matrices L, M, and N in the implicit calculation [Eq. (3)] are obtained using perfect gas relations only.

Validation

A Navier–Stokes code has been developed based on the numerical algorithm described earlier. The code has been val-

Table 1 Constants used in the definition of the grid

Grid type	$i_{max}v$	$j_{max}v$	$\Delta\bar{r}_{min} \times 10^5$	$\Delta\bar{r}_1$	$\Delta\bar{r}_2$	$j1$	$j2$	R_{outer}
CD	40	161	$1.42/R_{outer}$	$0.046/R_{outer}$	$2.8/R_{outer}$	50	100	3.2
CI	40	161	$0.71/R_{outer}$	$0.046/R_{outer}$	$2.8/R_{outer}$	50	100	3.2
CJ	40	175	$0.492/R_{outer}$	$0.0243/R_{outer}$	$1.11/R_{outer}$	50	100	2.25

Table 2 Stagnation point pressure comparison (perfect gas)

			p_{stag}/p_∞	
M_∞	Re_∞	T_w	Present	Exact
4.6	5000	3.3293	27.66	27.71
6.0	10^6	3.3293	46.87	46.81
6.0	10^6	2.0000	46.88	46.81
6.0	10^6	Adiabatic	46.87	46.81
8.0	10^6	Adiabatic	82.91	82.87
8.0	5×10^6	Adiabatic	82.91	82.87
8.0	10^7	Adiabatic	82.87	82.87
10.0	10^6	Adiabatic	128.8	129.2

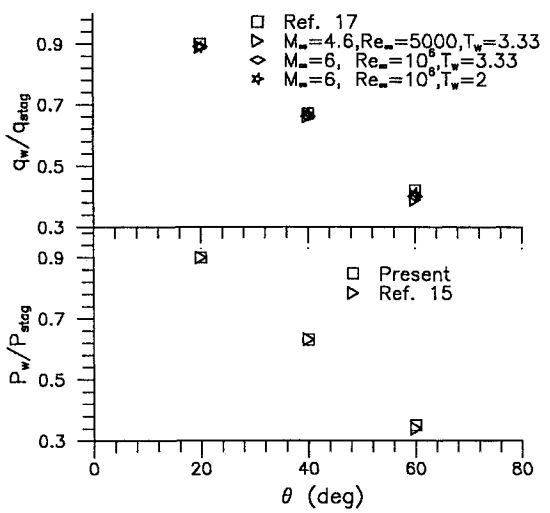

Fig. 2 P_w/P_{stag} and q_w/q_{stag} comparison.

idated for various cases involving different geometries, flow, and wall conditions. The details of the validation done with respect to flat plate have been reported.[2] In this article validation results will be confined to hemicylinder only. The grid is stretched in the direction normal to the hemicylinder surface and uniform grid spacing is used along the surface. The following stretching function is used:

$$\Delta\bar{r} = \tfrac{1}{2}\Delta\bar{r}_{min} \quad \text{if} \quad j = 1 \tag{9}$$

$$\Delta\bar{r} = \Delta\bar{r}_1(\Delta\bar{r}_{min}/\Delta\bar{r}_1)^{(j-1)/(j1-1)} \quad \text{if} \quad 1 < j \leq j1 \tag{10}$$

$$\Delta\bar{r} = \Delta\bar{r}_2(\Delta\bar{r}_1/\Delta\bar{r}_2)^{(j2-1)/(j2-j1-1)} \quad \text{if} \quad j1 < j \leq j2 \tag{11}$$

$$\Delta\bar{r} = \Delta\bar{r}_2 \quad \text{if} \quad j2 < j \leq j_{max}v - 1 \tag{12}$$

where $\bar{r}$ is the distance measured along η and normalized with respect to the normal distance between the body surface and the outer boundary, j is the grid index in the η direction, and $j_{max}v$ is the maximum number of cell vertices. Table 1 gives the values of various quantities used. In this table, R_{outer} is the radius of the outer boundary and $i_{max}v$ is the number of cell vertices in the ξ direction. These grids were obtained after making a thorough grid refinement study along the lines of Blottner[14] for a typical flow condition used in the present work. It was found that the errors, in pressure and temperature, for the grids chosen are less than 5%, and hence, the grids are considered adequate.

Table 3 Comparison of stagnation point heat transfer rate

			$\dot{q}_{stag}$	
M_∞	Re_∞	T_w	Reference 16	Present
4.6	5000	3.3293	0.692×10^{-2}	0.7274×10^{-2}
6.0	10^6	3.3293	0.819×10^{-3}	0.8996×10^{-3}
6.0	10^6	2.0	1.062×10^{-3}	1.1110×10^{-3}

Table 4 Comparison of the compressibility factor

Temperature, K	Reference 18	Present
2,000	1.00	1.0094
4,000	1.22	1.2005
8,000	2.00	2.0300
10,000	2.17	2.2000
12,000	2.71	2.7300
15,000	3.66	3.6700

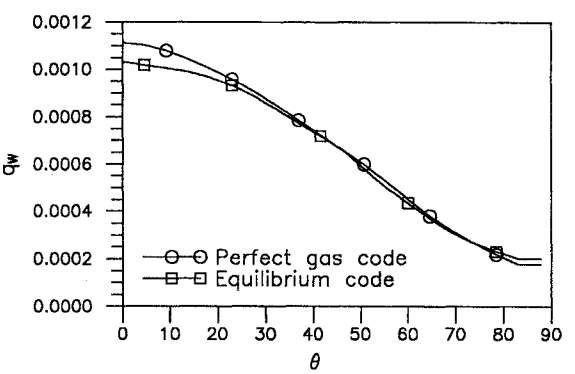

Fig. 3 Heat transfer rate distribution ($M_\infty = 6$, $Re_\infty = 10^6$, $T_w = 2$, no transpiration).

In Table 2, the stagnation point pressure computed from the Navier–Stokes code is presented along with the exact pressure obtained through the normal shock and the isentropic compression process. The present code predicts the pressure very accurately. In Fig. 2, p_w/p_{stag} values are compared for three locations along the hemicylinder surface with the values obtained by Tannehill.[15] The pressure distribution around the cylinder also agrees well as can be seen from this figure. The stagnation point heat transfer rate is compared with the Fay and Riddell[16] expression in Table 3 for perfect gas. The agreement between the two is within 10% of the Fay and Riddell value and can be considered fairly good. In Fig. 2, the quantity $\dot{q}_w/\dot{q}_{stag}$ is compared with the experimental results of Koppenwallner[17] at three locations around the hemicylinder and found to agree well. Though the experimental conditions of Koppenwallner are different, $\dot{q}_w/\dot{q}_{stag}$ is almost independent of the freestream and wall conditions, which is also evident from our results shown in Fig. 2.

The chemical equilibrium code is also validated for various cases. The chemistry model is validated separately by computing the compressibility factor and comparing this with the data obtained from Vincenti and Krugger[18] as shown in Table 4. There is a very good comparison between the two at all of the temperatures. The heat transfer rate distribution from the chemical equilibrium code is compared with that of perfect gas code in Fig. 3 for $M_\infty = 6$, $Re_\infty = 10^6$, and $T_w = 2$. At this

Mach number there will be no chemical reactions taking place. Still the results from the two codes differ to a certain extent because the chemical equilibrium code can take care of vibrational excitation, and hence, corresponds to a thermally perfect gas situation, whereas the perfect gas code assumes a calorically perfect gas model. Differences can also come because of the way in which the transport properties are evaluated in the two codes. From Fig. 3, it can be seen that the two results agree very well in regions away from the stagnation point. In the stagnation point region, the chemical equilibrium code shows lesser heat transfer rate. This difference is expected because it is in this region the vibrational excitation becomes significant. For $M_\infty = 6$, the stagnation point heat transfer rate obtained from the present work is 1.05×10^{-3} and that from the Fay and Riddell expression[16] is 1.08×10^{-3}. For $M_\infty = 10$ the corresponding values are 1.65×10^{-3} and 1.74×10^{-3}, respectively. In both cases the agreement is good. These values were computed for $Re_\infty = 10^6$ and $T_w = 2.0$. The temperature and density behind the normal shock was compared with that of Huber[19] and the difference was less than 1% for $M_\infty = 10$, $Re_\infty = 10^6$, and $T_w = 2$.

Results and Discussion

Transpiration cooling analysis has been made for $M_\infty = 6$, 8, 10, and $Re_\infty = 10^6$, 5×10^6 and 10^7. These parameters are chosen from a typical re-entry vehicle trajectory and the altitude corresponds to an altitude of 50 km. In view of the laminar calculations done in this work, Reynolds numbers chosen are on the higher side and in regions where the flow becomes turbulent the present results will be of academic interest only. Grid type CD has been used for a Reynolds number of 10^6 and grid type CI for Reynolds number of 5×10^6 or 10^7. Air is used as the transpirant and its initial temperature is assumed to be that of the freestream temperature. As mentioned earlier, the computations have been carried out for no net heat flow into the wall condition.[2,3] This condition implies that the aerodynamic heat flowing into the wall will be used up in raising the temperature of the coolant from its initial value T_c to the temperature at the wall T_w. Based on this condition [Eq. (2)] the wall temperature is determined.

Mass injection rate is a parameter in the present analysis, which can be fixed arbitrarily. A new method was devised[2] that alleviates the arbitrariness in fixing the mass injection rates. This method approximately determines the mass injection rates required to get a desired value of wall temperature and helps in fixing a relevant range for mass injection rates. Although the details are available in Refs. 2 and 4, the final form of the expression can be given as

$$\dot{m}_w = C_{h0}[K/(1 - K)] \tag{13}$$

where $K = (T_r - T_w)/(T_r - 1)$. The injection rates were calculated for different values of K (=0.2, 0.3, 0.4, and 0.5) at the stagnation point of the hemicylinder for $M_\infty = 6$ and $Re_\infty = 10^6$. The blowing rate is held constant over the entire surface. The same blowing rates are also used for other Mach numbers. The maximum blowing rate $\dot{m}_w$ corresponding to the value of $K = 0.5$ is 2.2×10^{-3}.

Effect of Blowing on Wall Temperature

In Fig. 4, the effect of gas injection on the wall temperature is presented for different blowing rates at $M_\infty = 8$ and $Re_\infty = 5 \times 10^6$. When there is no transpiration, the surface attains the adiabatic wall temperature. This temperature decreases slightly along the surface as can be seen from the figure. Because of blowing, the wall temperature decreases significantly. The effect of blowing on temperature is more pronounced away from the stagnation point. This can be explained as follows: from Eq. (2) it can be observed that for a given blowing rate the wall temperature will be higher if the aerodynamic heating is higher. Since the heat transfer to the surface is maximum at the stagnation point, wall temperature is also maximum at that point. Also the heat blockage effect because of gas injection is more significant in regions away from the stagnation point since the gas injected upstream of these points also influences the heat transfer at these points. It was observed in the case of a flat plate[2,3] that the gas injection had no effect on the wall temperature at the leading edge. Contrary to this it can be observed from Fig. 4 that in the case of hemicylinder all of the regions are significantly affected by blowing, including the stagnation point.

Relative Change in Temperature (E_T)

The relative change in temperature can be defined as the change in the wall temperature because of blowing with respect to the temperature when there is no blowing. Mathematically,

$$E_T = (T - T_0)/T_0 \tag{14}$$

where T is the temperature on the surface of the hemicylinder with blowing and T_0 is that without blowing. In Fig. 5, E_T vs θ is plotted for various freestream and blowing conditions. For all of the cases E_T is negative, indicating that the wall temperature decreases because of blowing. Although the effect of Mach number (in the range considered) is not very significant on E_T, particularly at lower blowing rates, the figure shows that the transpiration cooling becomes relatively less effective at higher Mach numbers. The effect of Reynolds number is very strong on E_T at all blowing rates and E_T decreases sig-

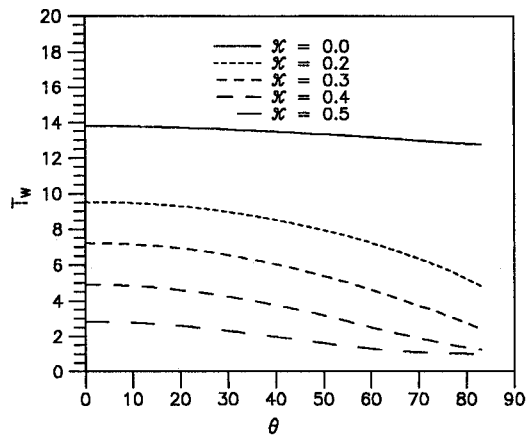

Fig. 4 Temperature variation on the surface ($M_\infty = 8$ and $Re_\infty = 5 \times 10^6$).

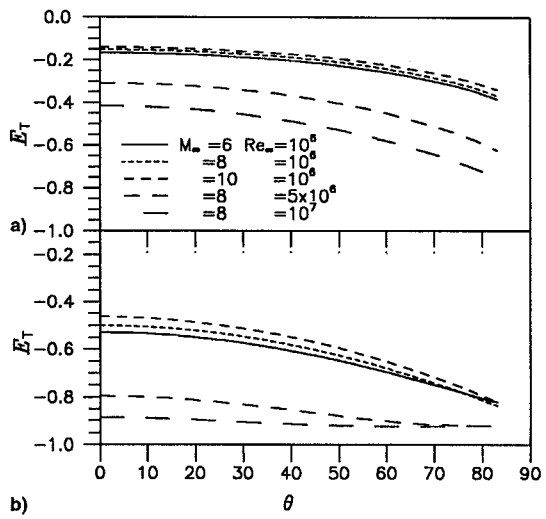

Fig. 5 Relative change in temperature. K = a) 0.2 and b) 0.5.

nificantly with increasing Reynolds number. It can be seen from Fig. 5 that at higher blowing rates and Re_∞, E_T is reduced to its limiting value in some regions of the hemicylinder. There is a limit to the value of E_T since there is a limit to the minimum temperature attainable, which is determined by the initial temperature of the coolant T_c, as per Eq. (2). Unlike the case of flat plate, E_T cannot be correlated to the local Re in this case.

Estimated Temperature Analysis

In Ref. 2, the mechanism of transpiration cooling was classified into two phases: preinjection and postinjection. In the preinjection phase, the coolant that is initially at a temperature T_c will absorb some of the heat coming into the wall even before injection. In the postinjection phase, the injected coolant reduces the heat generated in the boundary layer by altering its characteristics. In most of the earlier studies on transpiration cooling, the preinjection phase was not considered. Instead the surface temperature was always assumed to be known and the effect of injection of coolant at this temperature on the heat generated in the boundary layer was studied. In the present study, the preinjection phase of transpiration cooling has also been accounted for by using the no net heat transfer to the wall condition. The wall temperature acquired under such a condition is because of the effect of both phases. To assess the magnitude of the postinjection phase of cooling, the temperature of the wall is estimated in the absence of postinjection phase of cooling and this is compared with the actual wall temperature. The final expression for the estimated temperature[4] can be given as

$$T_w^{\text{est}} = \frac{\dot{m}_w T_c + C_{h0} T_r}{\dot{m}_w + C_{h0}} \tag{15}$$

In Fig. 6, the ratio T_w/T_w^{est} is plotted for different freestream and blowing conditions. Considering the curve corresponding to $M_\infty = 6$ and $Re_\infty = 10^6$, it can be seen that the ratio T_w/T_w^{est} remains close to unity at lower blowing rates, indicating that the postinjection phase of cooling is negligible at lower blowing rates. At higher blowing rates this value reduces substantially all over the surface with larger reduction occurring away from the stagnation point. This indicates that the postinjection phase of cooling becomes important as the blowing rate is increased, which is expected. What is significant is that, unlike the flat plate,[2,3] the postinjection phase of cooling becomes important over the entire surface. Figure 6 shows that the effect of M_∞ is insignificant at lower blowing rates, and at higher blowing rates the postinjection cooling effect decreases with increase in M_∞. Re_∞ influences the postinjection cooling very strongly as can be seen from the figure. At higher Re_∞, postinjection cooling becomes important, even at lower blowing rates. In fact the figure shows that the stagnation point temperature is only 35% of the temperature in the absence of postinjection cooling.

Velocity and Temperature Profiles

In Fig. 7, velocity and temperature profiles are plotted at $\theta = 83$ deg for various blowing rates and for $M_\infty = 8$ and $Re_\infty = 5 \times 10^6$. The increase in the momentum boundary-layer thickness because of blowing can be seen in Fig. 7a. Though the effect of blowing on skin-friction coefficient is not presented in this article, it was not found that the relative change in the skin-friction coefficient closely follows that of wall temperature.[4] In Fig. 7b the temperature profiles are shown. When there is no gas injection, the temperature profile corresponds to the adiabatic wall case. As the blowing rate is increased, the structure of the boundary layer is changed and a positive temperature gradient sets in. This is the result of the no net heat flow into the wall condition that is imposed. A further increase in the blowing rate decreases the wall temperature, and as the temperature approaches the initial temperature of the coolant the temperature gradient also tends to zero. This can be seen from the figure at $K = 0.5$.

Spatially Varying Mass Injection Rate

In the previous paragraphs, the effect of spatially constant mass injection on the wall temperature has been presented. It was found that the wall temperature decreases along the surface for spatially constant mass injection rate, implying that the mass injection rate should decrease along the surface for maintaining an isothermal wall. It is often desirable to have an isothermal wall from the structural design point of view to avoid thermal stresses. Hence, the mass injection rate distribution required for maintaining the surface at a particular temperature under no net heat flow condition [Eq. (2)] has been determined for $M_\infty = 10$ and $Re_\infty = 10^6$. This study has been made for three different wall temperatures ($T_w = 2$, 3.465, and 9.47). Figure 8 shows the results of such a computation. In Fig. 8a, the blowing $\dot{m}_w$ is plotted with θ for various temperatures. As expected, larger blowing rates are required near the stagnation point compared to other regions. Also, larger blowing rates were required to maintain the surface at a lower temperature. This is expected as the heat load will be larger at lower wall temperatures. The more interesting feature of this investigation can be seen from Fig. 8b where the normalized blowing rate ($\dot{m}_w/\dot{m}_{\text{stag}}$) is plotted against θ. For all of the wall temperatures, the data points practically fall on the same curve. This indicates that the normalized blowing rate distribution is

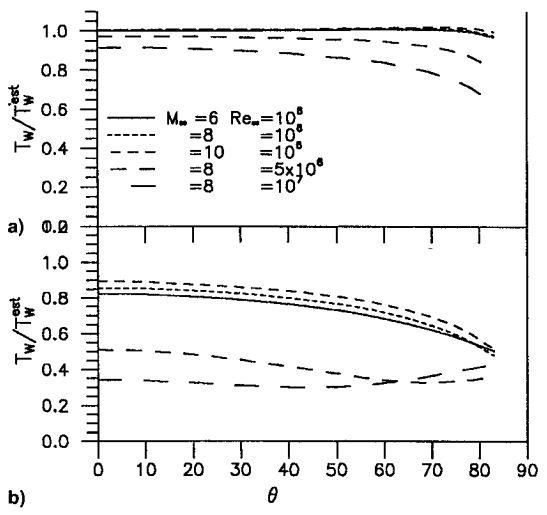

Fig. 6 Estimated temperature variation. K = a) 0.2 and b) 0.5.

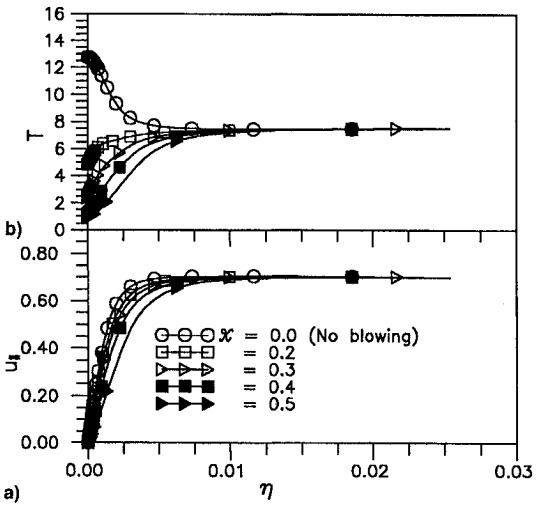

Fig. 7 Velocity and temperature profiles for $M_\infty = 8$ and $Re_\infty = 5 \times 10^6$.

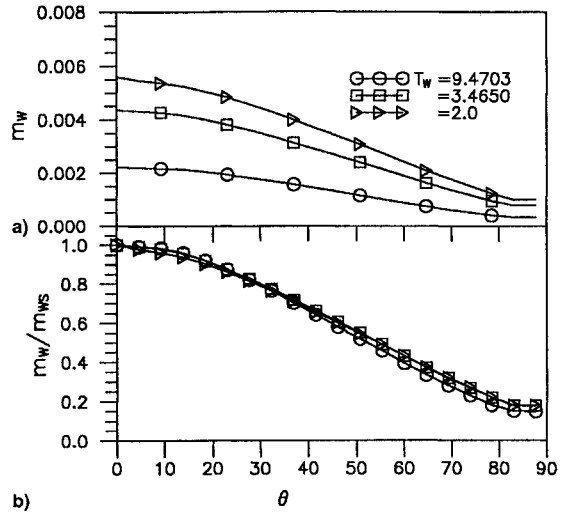

Fig. 8 Blowing rate variation of a) m_w with θ and b) m_w/m_{ws} with θ.

independent of the wall temperature. To determine the blowing rate required at any point it is only needed to correlate the blowing rate required at the stagnation point with temperature and $\dot{m}_w/\dot{m}_{stag}$ with θ.

Equilibrium Chemistry

Computations have been made for two freestream Mach numbers (6 and 10) with $Re_\infty = 10^6$. In both cases, an isothermal wall is assumed at a temperature $T_w = 2$. The blowing rate distribution required for maintaining such an isothermal wall is determined in both cases. In Fig. 9, the result of these computations is shown along with that of perfect gas computation. As the Mach number is increased, the blowing rate requirement also increases substantially as can be seen in Fig. 9a. This is expected since the adiabatic wall temperature is higher at higher Mach numbers and larger cooling is required to bring down the temperature to a value of 2. Comparing the blowing rate requirements for perfect gas and chemically equilibrium flows at $M_\infty = 10$, it can be seen that a much higher blowing rate is required when the flow is in chemical equilibrium. This is true in spite of the fact that the recovery temperature is smaller for chemical equilibrium flows. One reason can be given for this: gas injection is effective in reducing the conductive heating. In a perfect gas case, since no concentration gradient exists, the entire heat flow into the wall is because of the heat conduction. This gets significantly affected because of the gas injection. On the other hand, in the chemically equilibrium flows, the total heat flow into the wall is because of both conductive heating and mass diffusion arising out of concentration gradients. Since the gas injection affects only the conductive part, its net effect on the total heat transfer rate is much less compared to that of the perfect gas. This probably explains the larger blowing rates required in the case of chemically equilibrium flows. In Fig. 9b, the normalized blowing rates are plotted against θ. Comparing the perfect gas results with the chemically equilibrium case, it is observed that not only the magnitude of the blowing rates is different (as seen from Fig. 9a), but even the blowing rate distribution is different. From Fig. 9b, it can also be seen that the normalized blowing rate distribution is more or less independent of the freestream Mach number.

In a previous section the blowing rate distribution required to maintain an isothermal wall at $T_w = 2$ under conditions of no net heat flow into the wall was determined. These results have been obtained from the code by imposing an isothermal wall condition and adjusting the blowing rate at every time step such that Eq. (2) is satisfied. This leads to a steady state with some blowing rate distribution. One can think of another computation in which the same freestream conditions, the wall temperature, and the steady-state blowing rate of the previous computation are used, but without imposing Eq. (2). The latter one represents the kind of analysis that researchers have done in the past. The steady-state results from the latter computation will be exactly the same as the former computation since the freestream, wall, and the geometric conditions are the same for both. Hence, the heat transfer rate into the wall obtained from the former computations can be analyzed and can be interpreted as the heat transfer rate into the wall under conditions of a given blowing rate distribution, wall temperature, and freestream conditions. With this argument, the results of heat transfer from the former computations are presented in Fig. 10. Figure 10a shows that the heat transfer rate is slightly higher for chemical equilibrium flows than for the perfect gas when there is no transpiration. In Fig. 10b the same results are shown with transpiration cooling. Note that the blowing rate distributions used for both cases are different. The blowing rate distributions correspond to the ones shown in Fig. 9a. From Fig. 10b one aspect is clear, that in spite of having a much larger blowing rate, the heat transfer rate in the case of chemical equilibrium flows is larger than that for the perfect gas that supports the arguments made in a previous section. Figure 11 shows the ratio ψ of the heat transfer rate with and without transpiration cooling. This figure shows that even with larger blowing rates the ψ is larger for chemical equilibrium

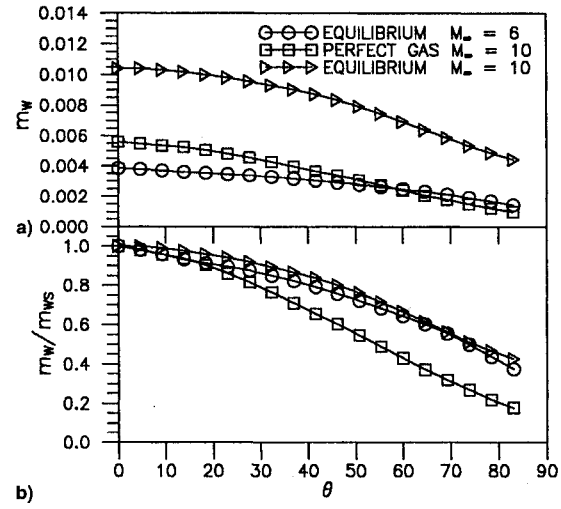

Fig. 9 Blowing rate variation around hemicylinder ($Re_\infty = 10^6$ and $T_w = 2$).

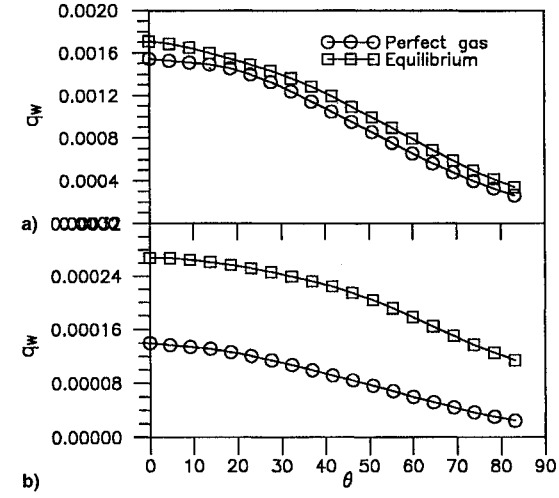

Fig. 10 Heat transfer variation along the surface ($M_\infty = 10$ and $Re_\infty = 10^6$): a) no transpiration and b) with transpiration.

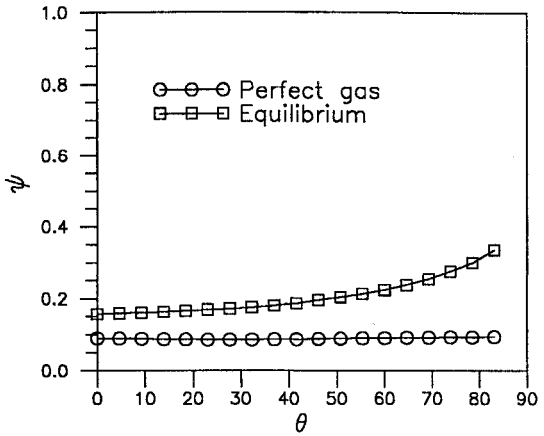

Fig. 11 Heat transfer reduction because of blowing (M_∞ = 10, Re_∞ = 10^6 and T_w = 2).

flows. This indicates that the transpiration cooling becomes less effective in chemical equilibrium flows than in perfect gas flows.

Conclusions

The results of transpiration cooling analyses made for flow over a hemicylinder were discussed. Injecting cold air was found to be effective in reducing the wall temperature. When the spatially constant injection rate was used, the effect of gas injection was nonuniform along the hemicylinder. The effect of Mach number on cooling effectiveness was found to be insignificant, whereas the Reynolds number had a significant effect. The postinjection phase of cooling became significant only at larger blowing rates. It was found necessary to decrease the mass injection rate along the hemicylinder to maintain an isothermal wall. Also, the normalized blowing rate distribution was found to be independent of the wall temperature. Transpiration cooling was found to be less effective for chemical equilibrium flows compared to the perfect gas flows.

References

[1]McConarty, W. A., and Anthony, F. M., "Design and Evaluation of Active Cooling Systems for Mach 6 Cruise Vehicle Wings," NASA CR-1916, 1971.

[2]Sreekanth, and Reddy, N. M., "Transpiration Cooling Analysis at Hypersonic Mach Numbers Using Navier-Stokes Equations," AIAA Paper 94-2075, June 1994.

[3]Sreekanth, and Reddy, N. M., "Study of Transpiration Cooling over a Flat Plate at Hypersonic Mach Numbers," *Journal of Thermophysics and Heat Transfer*, Vol. 9, No. 3, 1995, pp. 552–554.

[4]Sreekanth, "Transpiration Cooling Analysis at Hypersonic Mach Numbers Using Navier-Stokes Equations," Ph.D. Dissertation, Indian Inst. of Science, Bangalore, India, Dec. 1993.

[5]Van Leer, B., "Flux-Vector Splitting for Euler Equations," Inst. for Computer Applications in Science and Engineering, Rept. 82-30, 1982.

[6]Anderson, W. K., Thomas, J. L., and Van Leer, B., "A Comparison of Finite Volume Flux Vector Splittings for Euler Equations," AIAA Paper 85-0122, 1985.

[7]Peyret, T., and Taylor, T. D., *Computational Methods for Fluid Flow*, Springer–Verlag, New York, 1983, pp. 108–112.

[8]Liou, M. S., and Hsu, A. T., "A Time Accurate Finite Volume High Resolution Scheme for Three-Dimensional Navier-Stokes Equations," AIAA Paper 89-1994, 1989.

[9]White, F. M., *Viscous Fluid Flow*, McGraw–Hill, New York, 1974.

[10]Svehla, R. A., "Estimated Viscosities and Thermal Conductivities of Gases at High Temperatures," NASA TR R-132, 1962.

[11]Anderson, J. D., *Hypersonic and High Temperature Gas Dynamics*, McGraw–Hill, New York, 1989, pp. 591–609.

[12]Liou, M. S., Van Leer, B., and Shuen, J. S., "Splitting of Inviscid Fluxes for Real Gases," *Journal of Computational Physics*, Vol. 87, No. 1, 1990, pp. 1–14.

[13]Tannehill, J. C., and Mugge, P. H., "Improved Curve Fits for the Thermodynamic Properties of Equilibrium Air, Suitable for Numerical Computation Using Time-Dependent or Shock-Capturing Methods," NASA CR-2470, Oct. 1974.

[14]Blottner, F. G., "Accurate Navier-Stokes Results for the Hypersonic Flow over a Spherical Nose Tip," *Journal of Spacecraft and Rockets*, Vol. 27, No. 2, 1990, pp. 113–122.

[15]Tannehill, J. C., Holst, T. L., and Rakich, J. V., "Numerical Computation of Two-Dimensional Viscous Blunt Body Flows with an Impinging Shock," *AIAA Journal*, Vol. 14, No. 2, 1976, pp. 204–211.

[16]Fay, J. A., and Riddell, F. R., "Theory of Stagnation Point Heat Transfer Dissociated Air," *Journal of Aerospace Sciences*, Vol. 25, No. 2, 1958, pp. 73–85.

[17]Koppenwallner, G., "Fundamentals of Hypersonics: Aerodynamics and Heat Transfer," *Hypersonic Aerothermodynamics*, von Kármán Inst. for Fluid Dynamics, Belgium, 1984.

[18]Vincenti, W. G., and Kruger, C. H., *Introduction to Physical Gas Dynamics*, Wiley, New York, 1965.

[19]Huber, P. W., "Hypersonic Shock-Heated Flow Parameter for Velocities to 46000 Feet per Second and Altitudes to 323000 Feet," NASA TR R-163, Dec. 1963.